Kinetic and computational studies of the composition and structure of activated complexes in the asymmetric deprotonation of cyclohexene oxide by a norephedrine-derived chiral lithium amide †

2 PERKIN

Daniel Pettersen, Mohamed Amedjkouh, Sten O. Nilsson Lill, Kristian Dahlén and Per Ahlberg *

Organic Chemistry, Department of Chemistry, Göteborg University, SE-412 96, Göteborg, Sweden. E-mail: Per.Ahlberg@oc.chalmers.se; Fax: +46 31 772 2899; Tel: +46 31 772 2899

Received (in Cambridge, UK) 20th February 2001, Accepted 19th March 2001
First published as an Advance Article on the web 27th April 2001

Rational design of efficient chiral lithium amides for enantioselective deprotonations demands understanding of the origin of the selectivity. The mechanism of deprotonation of cyclohexene oxide **1** by lithium (1*R*,2*S*)-*N*-methyl-1-phenyl-2-pyrrolidinylpropanamide **3**, which yields (*S*)-cyclohex-2-en-1-ol (*S*)-**5** in 93% enantiomeric excess in tetrahydrofuran (THF), has been investigated. Kinetics have been used to show that the reaction is first order with respect to the reagents **1** and **3**, respectively. NMR investigations of a ^{6}Li and ^{15}N labelled isotopologue of **3** have previously shown that **3** is mainly a dimer of the lithium amide monomer in THF in the initial state. On the basis of these results it is concluded that the rate-limiting activated complexes for the epoxide deprotonation are composed of two molecules of monomer of lithium amide **3** and one molecule of epoxide. Structures and energies of unsolvated and specific THF-solvated reagents and activated complexes have been calculated using PM3 and B3LYP/6-31+G(d). The results are currently being explored for the rational design of chiral lithium amides with improved stereoselectivities.

Introduction

Enantiomers of chiral lithium amides are used in asymmetric deprotonation of *e.g. meso*-epoxides to afford chiral allylic alcohols in enantiomeric excess (ee).[1–3] Such products are important intermediates in the total synthesis of *e.g.* biologically active compounds.[4–7] There is a need for invention of new chiral amides with improved stereoselectivities and which are easily available synthetically. The development of stereoselective lithium amides for deprotonations has mainly been carried out in a trial-and-error fashion.[8–17] To be able to rationally develop new and highly selective chiral lithium amides knowledge is needed about the detailed reaction mechanisms and, in particular, the composition and structures of the rate-limiting activated complexes involved.

By use of multinuclear NMR studies of isotopically labelled lithium amides the molecular composition of the lithium amide aggregates in the initial state has been determined. Such knowledge and transition state theory, together with kinetic reaction orders with respect to reactants in the deprotonation reaction, give the composition of the rate-limiting activated complexes.[18–20] Based on this it is possible to computationally model structures of initial state complexes and activated complexes in solution.[21–23] Such knowledge is a prerequisite for rational design by *e.g.* computational methods of new and highly stereoselective chiral lithium amides.

Previous investigations of the structure of activated complexes involved in the deprotonation of cyclohexene oxide **1** by lithium (*S*)-2-(pyrrolidin-1-ylmethyl)pyrrolidide **2** have shown that the rate-limiting deprotonation activated complexes are built from one molecule of lithium amide monomer and one molecule of **1**.[18,21] This was the starting point for the design of the norephedrine-derived chiral lithium amide lithium (1*R*,2*S*)-*N*-methyl-1-phenyl-2-pyrrolidinylpropanamide **3** and its enantiomer. An efficient synthesis of the corresponding precursor diamine (1*R*,2*S*)-*N*-methyl-1-phenyl-2-pyrrolidinylpropanamine **4** and its enantiomer was also developed.[24] Using lithium amide **3** or its enantiomer ees ≥93% of (*S*)-cyclohex-2-en-1-ol [(*S*)-**5**] or its enantiomer, respectively, were obtained upon deprotonation of **1**.

Independently O'Brien and co-workers have recently reported the synthesis of **4** and the application of the lithium amide **3** in enantioselective deprotonation of different functionalised *meso*-epoxides yielding allylic alcohols with high ees.[25,26]

In this paper we report a detailed study of the mechanism of the reaction shown in Scheme 1 in which **3** deprotonates **1** in

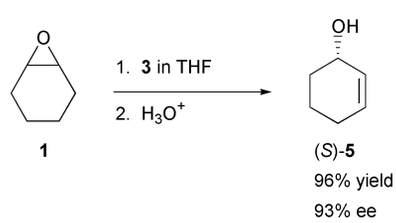

Scheme 1 The investigated enantioselective deprotonation reaction of the epoxide **1** by the lithium amide **3** in THF.

THF to yield after isolation the allylic alcohol (*S*)-**5** in 93% ee. A kinetic study at 20 °C has been carried out and the reaction orders with respect to **1** and **3** have been determined. A detailed computational study of amide initial state structures and possible activated complexes is also presented.

Results and discussion

In this section the kinetic study of the molecular composition of the rate-limiting deprotonation activated complexes is presented together with computationally modelled aggregates of

† Electronic supplementary information (ESI) available: structures and energies of possible diastereoisomeric activated complexes leading to (*R*)- and (*S*)-products. See http://www.rsc.org/suppdata/p2/b1/b101657l/

 DOI: 10.1039/b101657l

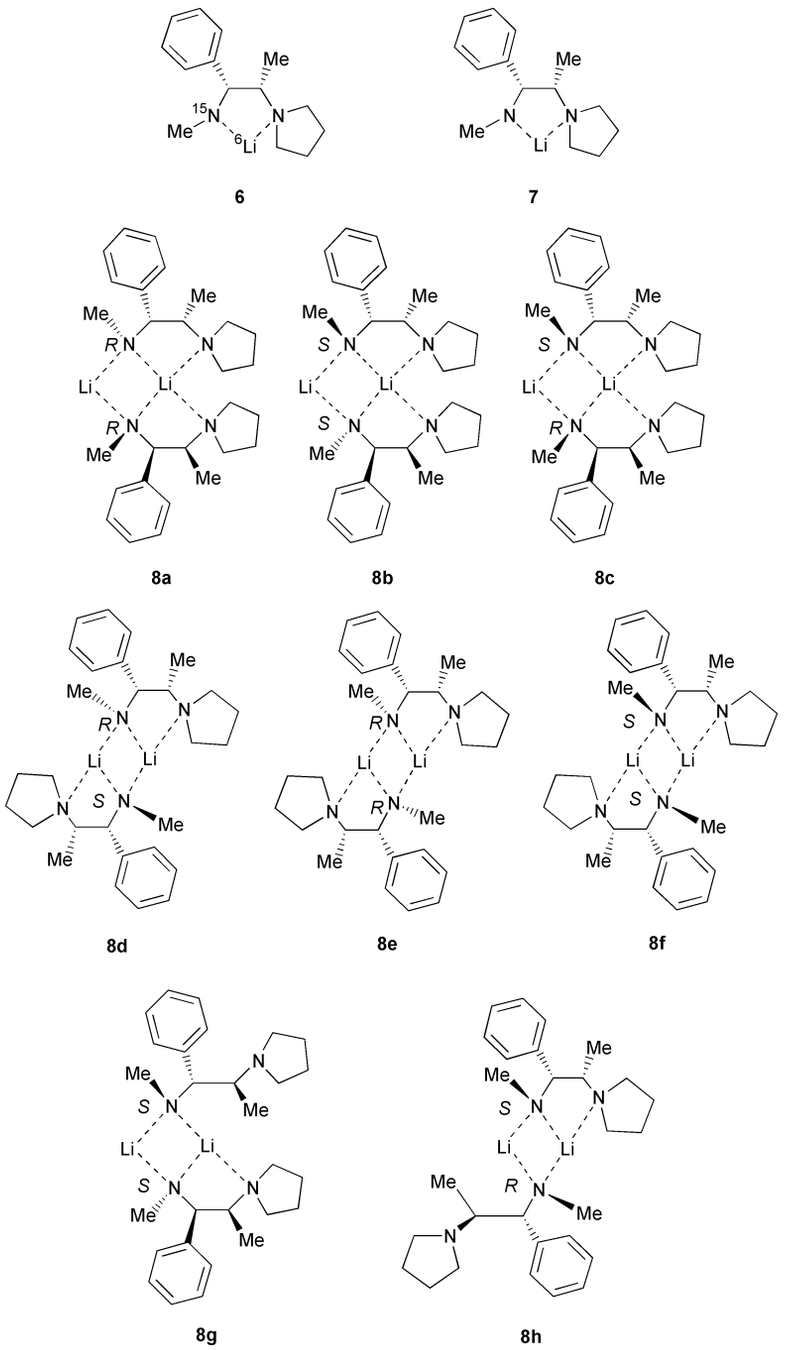

Fig. 1 Monomer structure and dimeric structures of **3**.

the lithium amide in the initial state and possible transition state structures.

Structure of the lithium amide in the initial state

The composition and structure of the lithium amide reagent **3** have been determined using its ^{6}Li and ^{15}N labelled isotopologue, of which its monomer **6** is shown in Fig. 1, and NMR coupling constants. The results have shown that in THF the lithium amide **3** is present mainly as a dimer with magnetically non-equivalent lithiums.[27] Other types of amide structures (monomer, trimer, tetramer, *etc*.) have not been detected.

Possible dimeric structures of **3**, excluding THF solvation, are shown in Fig. 1 together with a structure of monomer **7**. In isomers **8a**–**8c** the two lithiums are non-equivalent; one is dicoordinated and one is tetracoordinated. In the isomer **8d** the lithiums are also non-equivalent but both are tricoordinated. In the two structures **8e** and **8f** on the other hand the lithiums are both equivalent and tricoordinated.

The internal coordination bond between lithium and pyrrolidine nitrogen could be broken giving a structure such as **8g** with one lithium dicoordinated and one tricoordinated. Similarly **8f** yields **8h**. The isomerisation of dimers could proceed *via* structures with decreased internal coordination.

The NMR results are not conclusive with regard to which isomer with non-equivalent lithiums is dominant.

The enthalpies of formation and the structures shown in Fig. 1 with and without specific THF solvation have been calculated using the semiempirical computational method PM3.[28,29] This method was chosen because it has been shown to yield useful structures of lithium organic compounds and because the aggregates under scrutiny are computationally demanding. Several previous studies have shown the ability of PM3 to generate structures in good agreement with experimental results on lithium organic structures.[23,29–31] Optimisations have been performed with preceding conformational search with respect to the phenyl groups and solvent. The configurations of the nitrogens in the stereoisomeric dimers were also altered in the search

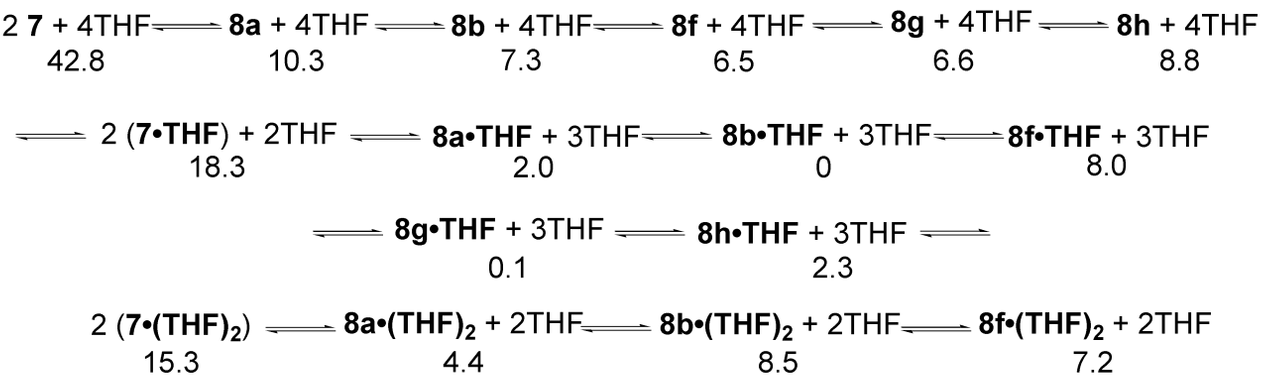

Scheme 2 Initial state equilibria between unsolvated and specific THF-solvated monomers and dimers and calculated enthalpies (kcal mol^{-1}) relative to **8b·THF** + 3 THF.

to find the most stable ones. Large variations in energy were found. The equilibria between monomer and dimers have also been studied including specific solvation by THF. In Scheme 2 equilibria between some of the most stable unsolvated, monosolvated and disolvated species are shown together with calculated relative enthalpies of formation.

Unsolvated and monosolvated dimers are both strongly favoured over unsolvated and monosolvated monomers. The dimeric complex calculated to be most stable is the THF-solvated dimer **8b·THF** in which THF is bonded to the tricoordinated lithium while the other lithium is intramolecularly tetracoordinated. However, **8g·THF** is only 0.1 kcal mol^{-1} higher in energy than **8b·THF**. This indicates that steric strain is released when the the pyrrolidine nitrogen coordination bond is broken. Disolvation by THF is found to be destabilising compared with their monosolvated counterparts.

The calculated structures of the stable dimers **8b·THF**, **8g·THF** and **8h·THF**, respectively, are shown in Fig. 2. Thus the computational results are consistent with our NMR findings that dimers with non-equivalent lithiums are more abundant than ones with equivalent lithiums. The isomerisation of dimeric structures with non-equivalent lithiums to structures with equivalent lithiums is probably rapid.

In the next section the kinetic determination of reaction orders with respect to reactants of the epoxide deprotonation is presented.

Kinetics

Knowledge of the lithium amide reagent **3** as being dimeric in the initial state in THF makes it possible to use the kinetics of the epoxide deprotonation to determine the composition of the rate-limiting activated complexes involved. To achieve this, the reaction orders of the reactants have to be experimentally determined. A general rate equation for product formation is shown in eqn. (1) with the reaction orders x and y with respect to the reagents **1** and **3**, respectively.

Taking the logarithm of eqn. (1) yields eqn. (2).

$$d[\mathbf{5}]/dt = k_{obs}[\mathbf{1}]^x\,[\mathbf{3}]^y \quad (1)$$

$$\log (d[\mathbf{5}]/dt) = \log k_{obs} + x\log [\mathbf{1}] + y\log [\mathbf{3}] \quad (2)$$

A calibrated quench-extraction-gas chromatography procedure described in the Experimental has been developed to determine initial rates (d[**5**]/dt). The time dependence of the concentration of the product **5** has been measured using different initial concentrations of the epoxide **1** and lithium amide **3**, respectively. Initial rates were used to determine reaction orders in order to avoid possible interference of reaction products. The asymmetric deprotonation of **1** by **3** was carried out in THF at 20.00 ± 0.05 °C. The reaction was started by addition of **1** to a solution of **3** and the reaction was monitored by measuring the appearance of extracted **5** at conversions of **1** usually lower than 5%. In Fig. 3 the concentration of **5** *vs.* time has been plotted. The initial rates were measured as the slopes of fitted straight lines. The runs were usually reproduced within <3% of the average values, respectively.

The determined initial rates at different initial concentrations of the reactants are collected in Table 1.

Using eqn. (2) reaction orders were determined from the slopes of fitted straight lines of plots of log (d[**5**]/dt) *vs.* log [**1**] and log [**3**] shown in Fig. 4 and 5, respectively. The determined slopes were 0.97 and 1.05 for **1** and **3**, respectively.

Thus, the deprotonation reaction is concluded, within experimental error, to be first order with respect to both the epoxide **1** and **3**, *i.e.*, first order in lithium amide dimer.

To be able to interpret the experimentally observed reaction orders these have been compared with predicted reaction orders for monomer- and dimer-based pathways. Reactions through the β-elimination activated complexes of types **9** and **10** (which are kinetic representatives for monomer- and dimer-based transition states, respectively) have been considered.

Activated complexes **9** are built from the monomer **7** of **3** and one molecule of **1**. The transition states **10** on the other hand are composed of two monomers (a dimer) of **3** and one epoxide molecule. Transition states **10a** to **10f** are built from one molecule of **1** and dimers **8a** to **8f**, respectively. According to transition state theory the activated complexes are assumed to be in equilibrium with the reagents **1** and **3**. The reaction *via* activated complex **9** is shown in eqn. (3) and reactions involving dimers in the activated complexes are described by eqn. (4).

$$0.5\,\mathbf{3} + \mathbf{1} \rightleftharpoons \mathbf{9} \rightarrow \mathbf{5} + \mathbf{4} \quad (3)$$

$$\mathbf{3} + \mathbf{1} \rightleftharpoons \mathbf{10} \rightarrow \mathbf{5} + 0.5\,\mathbf{3} + \mathbf{4} \quad (4)$$

From eqn. (3) and eqn. (4) and transition state theory the rate equations in eqn. (5) and eqn. (6) have been derived, respectively.

$$d[\mathbf{5}]/dt = k_1[\mathbf{3}]^{0.5}[\mathbf{1}] \quad (5)$$

$$d[\mathbf{5}]/dt = k_2[\mathbf{3}][\mathbf{1}] \quad (6)$$

Thus, if the deprotonation proceeds *via* rate-limiting activated complexes **9**, the reaction order will be 0.5 with respect to **3** [eqn. (5)] since the lithium amide has been shown to be dimeric in the initial state. On the other hand, if the reaction takes place *via* activated complexes **10**, which are all built from lithium amide dimers and one molecule of **1**, respectively, the reaction order is predicted to be 1 with respect to **3** [eqn. (6)]. Thus, in both cases the reaction order with respect to **1** will be 1. Clearly only the latter alternative [eqn. (6)] is consistent with the experimentally determined reaction orders. Thus, it is concluded that the rate-limiting activated complexes are composed of a lithium amide dimer and one molecule of the epoxide **1**. In the next section the computational modelling of structures and energies of possible transition states is presented.

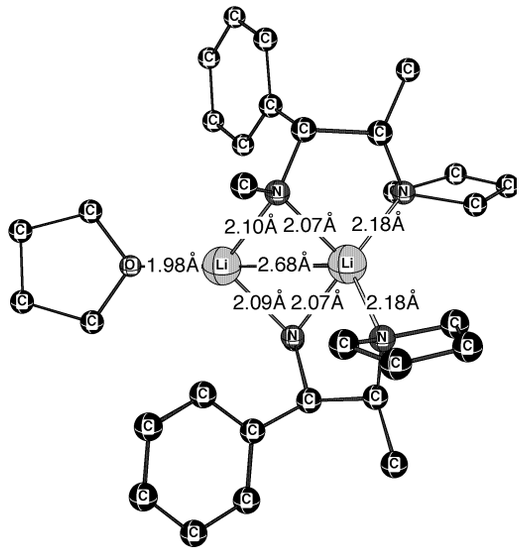

8b•THF

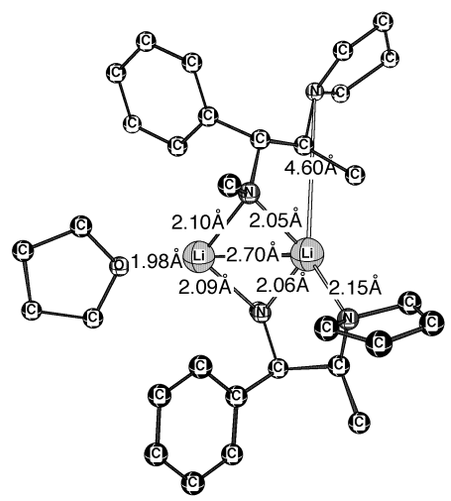

8g•THF

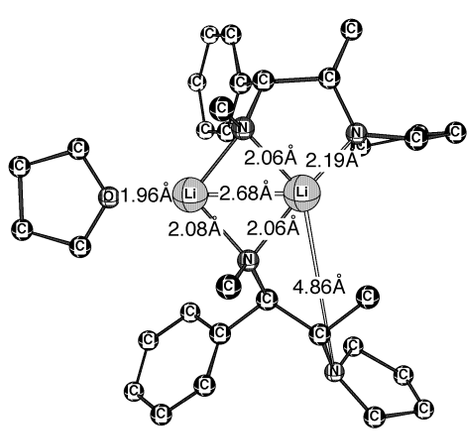

8h•THF

Fig. 2 The calculated most stable structures by PM3 of the lithium amide. Relative stabilities are shown in Scheme 2. Hydrogens are omitted for clarity.

Computational study of activated complexes

The acquired knowledge about the composition of the rate-limiting activated complex focused the efforts on computational modelling on dimer-based transition state structures. Monomer-based activated complexes have also been modelled. However, only *syn*-β-elimination activated complexes have been modelled in the absence of any evidence for α-elimination. Structures and energies of possible diastereoisomeric activated complexes leading to (*R*)- and (*S*)-products, respectively, have been calculated by PM3 and B3LYP/6-31+G(d). Altogether about 82 unsolvated, mono- and di-THF-solvated activated complexes have been calculated (see electronic supplementary information †). In Table 2 enthalpies of activated complexes having the lowest enthalpy are reported.

Table 1 Initial rates obtained from runs with different initial concentrations of **1** and **3** in THF at 20.00 °C

Run	[**1**]/mM	[**3**]/mM	(d[**5**]/d*t*)/10^6 M s^{-1}
1	200	50	8.97
2	200	50	9.19
3	200	65	13.4
4	200	100	19.5
5	200	100	20.1
6	200	130	24.6
7	20	100	2.08
8	50	100	5.13
9	60	100	6.30
10	60	100	6.67
11	100	100	10.3
12	100	100	10.2

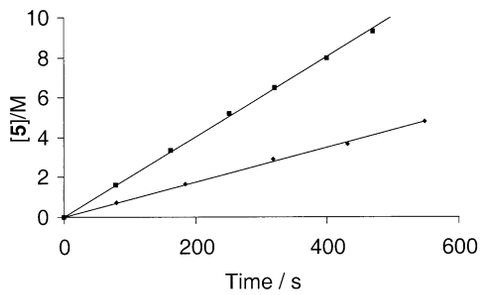

Fig. 3 The concentration of **5** plotted *vs*. time for the initial part of the deprotonation reaction of **1** is shown for two different initial concentrations of **1**: lower line 100 mM; upper line 200 mM.

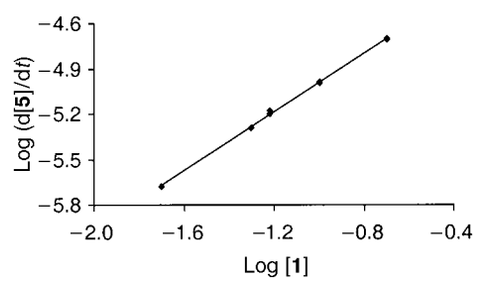

Fig. 4 log ([**5**]/d*t*) is plotted *vs*. log [**1**] and the slope of the fitted straight line is the measured order of the reaction with respect to the reactant **1**.

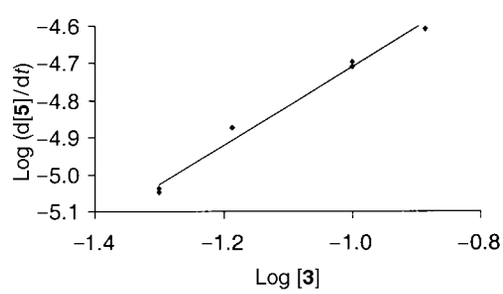

Fig. 5 log ([**5**]/d*t*) is plotted *vs*. log [**3**] and the slope of the fitted straight line is the measured order of the reaction with respect to reactant **3**.

Table 2 Calculated enthalpies (kcal mol^{-1}) of formation (PM3) for different types of unsolvated and THF-solvated diastereomeric transition states

Solvent	**9**	**10a**	**10f**	**10g**	**10h**
Unsolvated	(*R*) 20.630	(*R*) 25.772	(*R*) 20.282	(*R*) 21.326	(*R*) 28.974
	(*S*) 20.831	(*S*) 23.449	(*S*) 20.303	(*S*) 20.052	(*S*) —[d]
1 THF	(*R*) −36.629	(*R*) −30.593	(*R*) −32.920[a]	(*R*) −32.987[c]	(*R*) −25.097
	(*S*) −37.056	(*S*) −28.337	(*S*) −34.810[b]	(*S*) −32.476	(*S*) −31.778

[a] Absolute energy: −1868.68586 E_h. (*R*)-**10f·THF** is +1.36 kcal mol^{-1} less stable than (*S*)-**10f·THF** calculated using B3LYP/6-31+G(d)//PM3. [b] Absolute energy: −1868.68802 E_h calculated using B3LYP/6-31+G(d)//PM3. [c] Absolute energy: −1868.68418 E_h. (*R*)-**10g·THF** is +2.41 kcal mol^{-1} less stable than (*S*)-**10f·THF** calculated using B3LYP/6-31+G(d)//PM3. [d] Not found at PM3 level.

Table 3 Calculated enantioselectivities for different types of pairs of transition states using the data in Table 2. The ees have been estimated assuming that the difference of free energies of activation is equal to the difference of the enthalpies of formation for the activated complexes yielding the (*R*)- and (*S*)-products, respectively

Solvent	**9**	**10a**	**10f**	**10g**	**10h**	Exp.
Unsolvated	17% (*R*)	96% (*S*)	2% (*R*)	79% (*S*)	—	
1 THF	35% (*S*)	96% (*R*)	92% (*S*)	41% (*R*)	100% (*S*)	93% (*S*)
1 THF			82% (*S*)[a]			

[a] Calculated using B3LYP/6-31+G(d)//PM3.

Of the dimer-based, unsolvated activated complexes the calculated diastereoisomeric complexes (*R*)-**10f** and (*S*)-**10g** (Scheme 3) were found to have the lowest enthalpy.

Their calculated enthalpies relative to the reference (Scheme 3) were almost equal (31.6 and 31.4 kcal mol^{-1}, respectively, see Scheme 3) and 1.1 and 0.2 kcal mol^{-1} more stable than the second most stable couple of diastereoisomeric complexes (*R*)-**10g** and (*S*)-**10f**, respectively. Upon monosolvation by THF the transition states become stabilised and (*R*)-**10g·THF** and (*S*)-**10f·THF** are now the complexes with lowest enthalpy. These have a 2.1 and 3.7 kcal mol^{-1} lower barrier, respectively, than the unsolvated counterparts. (*R*)-**10f·THF** is of almost equal energy as (*R*)-**10g·THF**. The calculated enthalpies of solvation of (*R*)-**10g** and (*S*)-**10f** are 3.2 and 3.9 kcal mol^{-1}, respectively. The solvation energy for (*R*)-**10f** is 2.1 kcal mol^{-1}. Optimised structures of the transition states are given in Fig. 6.

Solvation of any of the mono-THF-solvated dimers by another THF molecule resulted in destabilisation. Such transition states are therefore not further considered in the present context.

Using the data in Scheme 3 product enantiomeric excesses in the deprotonations *via* the unsolvated and mono-THF-solvated activated complexes **9**, **10a**, **10f**, **10g**, and **10h** have been predicted and the results are shown in Table 3. Reactions through both **10a** and **10g** favour the product enantiomer (*S*)-**5** but the reaction through **9** and **10f** slightly prefers the other enantiomer (*R*)-**5**. Mono-solvation by THF of the transition states has dramatic effects with reversal of the enantioselectivities. Now the stereoisomer (*R*)-**5** is the strongly preferred enantiomer by the reactions *via* **10a·THF** and **10g·THF**, and (*S*)-**5** is the preferred one *via* **9·THF**, **10h·THF** and **10f·THF**—the activated complex with the lowest activation enthalpy. The calculated ee using the transition states with lowest enthalpy is 91%. The agreement of this latter predicted value with the experimental 93% ee may be fortuitous. However, good agreement between PM3-calculated and measured enantioselectivities has previously been reported.[21,22] The predictive power of PM3 in the present context could be due to major cancellation of errors in energies because of close structural similarity between the diastereoisomeric activated complexes. Single-point calculations using B3LYP/6-31+G(d) on PM3-optimised transition states were also performed. (*R*)-**10g·THF** was found to be 1.06 kcal mol^{-1} higher in energy than (*R*)-**10f·THF** at DFT-level in contrast to the result at PM3 level. The energy difference between (*R*)-**10f·THF** and (*S*)-**10f·THF** was lowered from 1.89 kcal mol^{-1} to 1.36 kcal mol^{-1}. This corresponds to an ee of 82% in favour of (*S*)-**5** also in agreement with the experimental value of 93%.

The solvation is expected to lower both the entropy and the enthalpy of activation. Depending on the magnitude of these changes and the temperature, the free energy of activation may either decrease or increase upon solvation. If the former is the case for activated complex **10f·THF**, it will have lower free energy than **10f** + THF and thus be the transition state mainly used in the enantioselective deprotonation together with **10g·THF**. In the latter situation **10f** and **10g** may be the pre-

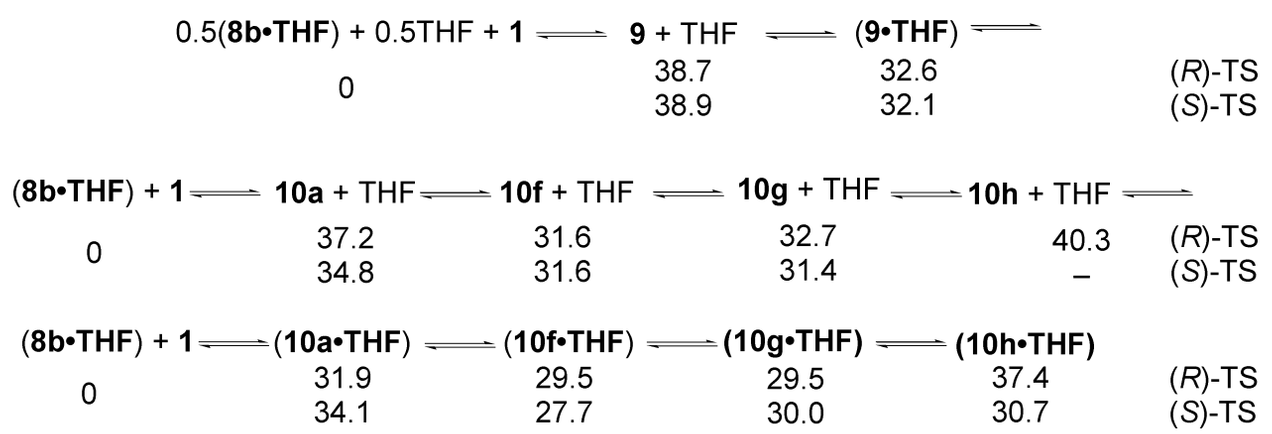

Scheme 3 Equilibria between initial states and possible unsolvated and specific THF-solvated activated complexes. Enthalpies are given in kcal mol^{-1}.

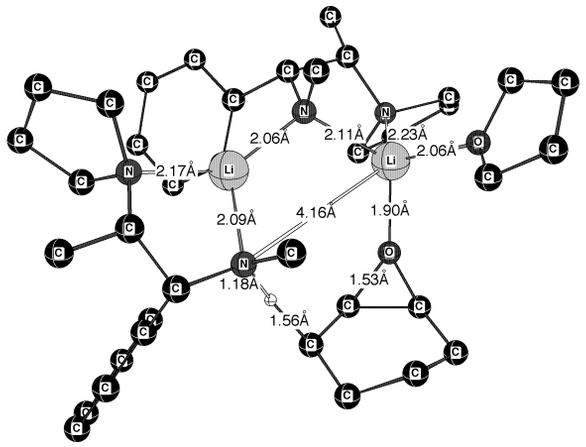

(*S*)-**10f•THF**

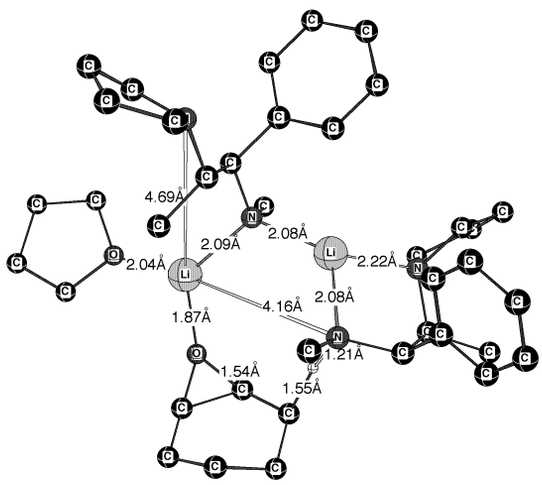

(*R*)-**10g•THF**

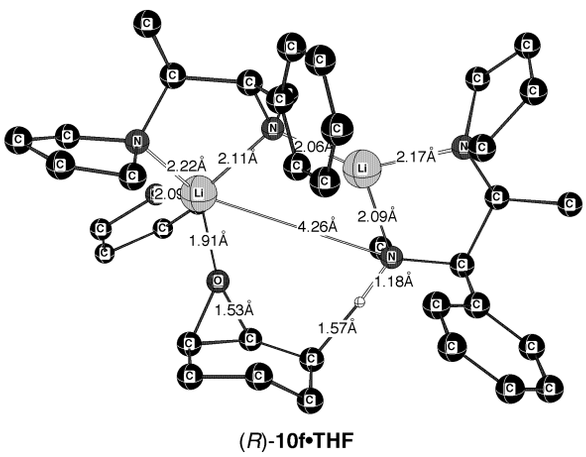

(*R*)-**10f•THF**

Fig. 6 The calculated most stable activated complexes by PM3. Relative stabilities are shown in Scheme 3. Some hydrogens are omitted for clarity.

dominating transition states depending on the concentration of THF. PM3 has been shown to underestimate solvation enthalpies by 3–4 kcal mol^{-1}.[21,31,32] Assuming an entropy of activation of about 5 kcal mol^{-1} a net stabilisation by solvation of (*S*)-**10f** is expected.[31,32] It is thus predicted that (*S*)-**5** will be the major enantiomer resulting from the chiral lithium amide deprotonation in line with what has been experimentally observed.

The THF-monosolvated dimer-based transition states (**10a·THF** and **10f·THF**) with lowest energy have been constructed using the dimers **8a** and **8f**, respectively (Fig. 1 and 6). These transition states may be seen as built from open dimers. **10g** was optimised by opening one lithium–pyrrolidine nitrogen bond in **10a**.

Along the reaction coordinate following coordination of the epoxide **1** to the dimer, one of the amide N–Li bonds opens. The lithium coordinates to the epoxide oxygen and the nitrogen that becomes basic abstracts a β-proton. As shown also in an earlier study of epoxide deprotonation using **2** the proton in flight in the transition state is found to be somewhat more than half-transferred towards the nitrogen from the carbon.[21] The C–O bond has opened up somewhat (1.53–1.54 Å) and the C–C double bond has started to develop (1.44–1.45 Å). Using **2** where the activated complexes were composed of monomers these bonds were found to be 1.52–1.55 Å and 1.45–1.46 Å, respectively, using PM3. These bond lengths are comparable to those of a recent high-level *ab initio* study (MP2/6-31+G(d)) of hydroxide deprotonation (no coordination of lithium to the epoxide oxygen) of **1** by Morgan and Gronert who found the corresponding distances to be 1.49 and 1.48 Å, respectively.[33]

The calculated barriers are somewhat higher (28 kcal mol^{-1}) than observed, which is a known error for PM3.[29,34]

Conclusion

The enantioselective deprotonation of the epoxide **1** by the lithium amide **3** in THF has been shown to proceed *via* rate-limiting transition states built from two monomers of **3** and one molecule of **1**. PM3 and B3LYP/6-31+G(d) calculations of structures and energies of possible activated complexes show the decisive role of THF solvation of the activated complexes for the enantioselectivity. The results suggest that proper structural modification of the activated complexes through structural modification of **3** may yield deprotonations with increased enantioselectivities.

Experimental

The synthesis of the lithium amide **3** precursor diamine (1*R*,2*S*)-*N*-methyl-1-phenyl-2-pyrrolidinylpropanamine **4** and its enantiomer (1*S*,2*R*)-*N*-methyl-1-phenyl-2-pyrrolidinylpropanamine from the commercially available enantiomers (1*R*,2*S*)-norephedrine and (1*S*,2*R*)-norephedrine, respectively, were carried out in three-step, one-pot preparations. In the first step the amino group in the norephedrine was transformed to a pyrrolidino group by reaction with 1,4-dibromobutane using a modification of a procedure reported by Zhao *et al.*[35] The second and third steps were carried out similarly to a recipe by Miao and Rossiter.[36] Upon mesylation of the hydroxy group an aziridinium ion intermediate formed. Reaction of the aziridinium ion with methylamine gave the amine **4**. The first step in the above sequence is a modification of a previously reported procedure by O'Brien and co-workers.[25]

Synthesis of (1*R*,2*S*)-*N*-methyl-1-phenyl-2-pyrrolidinylpropanamine 4

(1*R*,2*S*)-Norephedrine (6.0 g, 40 mmol), 1,4-dibromobutane (9.5 g, 44 mmol) and $NaHCO_3$ (7.4 g, 88 mmol) were refluxed in 100 ml toluene for 32 h. The solid was removed by filtration and the filtrate was concentrated *in vacuo* to yield the product tertiary amino alcohol as a colourless oil (97%). The oil was dissolved in dry THF (distilled from sodium–benzophenone ketyl) in a nitrogen atmosphere and the reaction flask was equipped with septa and cooled to 0 °C in an ice bath. Triethylamine (12.4 g, 120 mmol) was added to the stirred solution and methanesulfonyl chloride (9.35 g, 80 mmol) was added dropwise with a syringe over 20 min while a yellow precipitate formed. The reac-

tion flask was removed from the ice bath and stirred for another 1.5 h. Triethylamine (8.2 g, 80 mmol) and methylamine (30 ml, 240 mmol, 33% in ethanol) were added to the reaction mixture and the main part of the yellow precipitate dissolved. Water (10 ml) was then added and the remaining precipitate dissolved yielding a clear solution which was stirred at rt for 20 h. The aqueous phase was extracted with 3 × 40 ml diethyl ether. The collected organic phases were dried over Na_2SO_4 and filtered through 1.5 cm of silica to remove traces of amino alcohol. Evaporation *in vacuo* gave a brownish oil which was distilled at reduced pressure using a Vigreux to yield the amine **4** (6.6 g, 73%) as a colourless oil (>99% NMR). Bp 65–67 °C/3 × 10^{-2} mbar; δ_H (400 MHz; $CDCl_3$) 0.80 (3H, d, Me, J = 6.4 Hz), 1.75–1.83 (4H, m, CH_2), 1.90 (1H, br s, NH), 2.26–2.28 (1H, m, CHN, J = 3.2 Hz), 2.34 (3H, s, NMe), 2.54–2.57 (4H, m, NCH_2), 3.85 (1H, d, PhCHN, J = 3.2 Hz), 7.15–7.30 (5H, m, Ph). δ_C (125 MHz; THF-d_8) 13.4 (Me), 25.3 (CH_2), 35.8 (NHMe), 53.0 (NCH_2), 67.8 (CHN), 67.9 (CHN), 127.2, 128.7, 128.8, 143.3 (Ph). HRMS FAB (M + H) calculated $C_{14}H_{22}N_2$ 219.1861, found 219.1787.

Kinetics

General. Reaction vessels and syringes were dried in a vacuum oven (50 °C) overnight. Transfers of reagents were performed with gas-tight syringes in a nitrogen atmosphere. THF was distilled from sodium–benzophenone ketyl in a nitrogen atmosphere and stored over 4 Å molecular sieves in septum-sealed vials in a glovebox (Mecaplex GB 80 equipped with a gas purification system that removes oxygen and water). A stock solution (2.0 M) of cyclohexene oxide **1** (distilled from calcium hydride) in THF was prepared inside the glovebox. Hexan-1-ol was used as a standard in the GC-analysis; a stock solution (3.16 mM) of hexan-1-ol (distilled from calcium hydride) in carbon tetrachloride (distilled from calcium chloride) was prepared.

Determination of [BuLi]. A double Gilman titration following the (ASTM) standard E233-90 was used with some modifications. *n*-Butyllithium (1.0 ml, 2.5 M in hexanes) was added to hexane (10 ml) and the solution was quenched by addition of water (10 ml). Phenolphthalein (3 drops; 0.5 g l^{-1}, in ethanol–water 1 : 1) was added and the pink solution was titrated with hydrochloric acid (0.0902 M calibrated with NaOH) to colourlessness. A second sample of *n*-butyllithium (1.00 ml) was slowly added dropwise to a mixture of diethyl ether (2.5 ml, distilled from sodium–benzophenone ketyl) and benzyl chloride (1.00 ml, distilled from P_2O_5) under a nitrogen atmosphere. Water (10 ml) was added and the pink solution was titrated with hydrochloric acid (0.0902 M calibrated with NaOH) to colourlessness. The concentration of the *n*-butyllithium solution was calculated from the difference between the two titrations and was found to be 2.45 M.

Gas chromatography analysis. Gas chromatography analyses were performed on a Varian 3400 chromatograph equipped with an 8200 Cx autosampler and a flame ionisation detector (FID). For the separation an achiral DBWX-30W column (30 m, 0.25 μm) from J & W Scientific was used with hydrogen as carrier gas (2 ml min^{-1}). Reaction samples (1.0 μl) were introduced on to the column *via* a split injector (split flow 15 ml min^{-1}) and the components were separated using a temperature program. Initially the temperature was held at 80 °C for 2 minutes and then during 2 minutes it was increased to 120 °C. The injector temperature was 225 °C and the detector was held at 250 °C.

Gas chromatography response factors for **1** and **5** were determined using hexan-1-ol as a reference. Carbon tetrachloride samples of known compositions similar to those used in the kinetic experiments were analysed. The response factors and retention times measured were 1.01 and 2.3 min for cyclohexene oxide **1** and 0.85 and 4.9 min for cyclohex-2-en-1-ol **5**, respectively. The retention time for the reference compound hexan-1-ol was 3.8 min.

The enantiomeric excesses of **5** were measured using a Chrompack Chirasil-CB Dex (30 m, 0.25) at 90 °C. $t_R(S)$-**5** = 7.45 min, $t_R(R)$-**5** = 7.90 min.

Typical kinetic procedure. Amine **4** (43.7 μl, 0.2 mmol) was dissolved in THF (775 μl) in a reaction vessel inside the glovebox and then transferred out of the glovebox, and *n*-butyllithium (81.5 μl, 2.45 M in hexanes) was added under a nitrogen atmosphere. The yellow reaction solution was allowed to equilibrate at 20.00 ± 0.05 °C for 10 minutes in a thermostat (Heto Birkerød). The reaction was started by addition of cyclohexene oxide **1** (100 μl, 2.0 M) and samples (50 μl) were withdrawn from the reaction vessel at approximately 2 minute intervals and quenched in hydrochloric acid solution (100 μl, 0.6 M saturated with sodium chloride). Compounds **1** and **5** were extracted with carbon tetrachloride (500 μl) containing the standard hexan-1-ol (3.16 mM). The liquid phases were separated by centrifugation and 250 μl of the organic phase were transferred to a vial and analysed by capillary gas chromatography.

The quantitative transfer of **1** and **5** from the aqueous phase to the carbon tetrachloride phase during the work-up was determined as follows: Solutions of hexan-1-ol and **5** in THF with compositions similar to those in the kinetic experiments were prepared. Samples (50 μl) were withdrawn and added to solutions of carbon tetrachloride (500 μl) containing hexan-1-ol (3.16 mM). Other samples (50 μl) of solutions of **1** and **5** were added to solutions of hydrochloric acid (100 μl, 0.6 M saturated with sodium chloride). The latter mixtures were extracted with solutions of carbon tetrachloride (500 μl) containing hexan-1-ol (3.16 mM). After separation by centrifugation 250 μl of the organic layers were transferred to vials. The samples from the two types of preparations were analysed by capillary gas chromatography. The concentration ratios of epoxide **1** and allylic alcohol **5** to hexan-1-ol determined for the two types of preparations were found to be within 0.5% of the average value, respectively.

The concentration of **5** was measured for about the first 5% of conversion of **1**. Initial rates were determined as the slopes of fitted straight lines to plots of concentrations of **5** *vs.* time (see Fig. 3). Initial rates were usually reproduced within 2% of the average values, respectively.

Computational details. Geometries were optimised at PM3 level of theory.[28] In Spartan[37] the option HHON[38] was used to correct for hydrogens in close contact.[39,40] All geometries were characterised as minima or transition states on the potential energy surface (PES) by use of the sign of the eigenvalues of the force constant matrix obtained from a frequency calculation. Transition states with exactly one imaginary frequency were confirmed to describe the correct movement on the PES by a mode analysis. Reaction energies and activation barriers were calculated at PM3 level of theory. Single point calculations using B3LYP/6-31+G(d)[41–45] were performed on selected transition states.

Acknowledgements

We thank the Swedish Natural Science Research Council for financial support and Mr Roine I. Olsson for discussions.

References

1 P. J. Cox and N. S. Simpkins, *Tetrahedron: Asymmetry*, 1991, **2**, 1.
2 D. M. Hodgson, A. R. Gibbs and G. P. Lee, *Tetrahedron*, 1996, **52**, 14361.
3 P. O'Brien, *J. Chem. Soc., Perkin Trans. 1*, 1998, 1439.
4 J. S. Sabol and R. J. Cregge, *Tetrahedron Lett.*, 1989, **30**, 3377.

5 T. Kasai, H. Watanabe and K. Mori, *Bioorg. Med. Chem.*, 1993, **1**, 67.
6 M. Asami, J. Takahashi and S. Inoue, *Tetrahedron: Asymmetry*, 1994, **5**, 1649.
7 S. Barrett, P. O'Brien, H. C. Steffens, T. D. Towers and M. Voith, *Tetrahedron*, 2000, **56**, 9633.
8 M. Kirihara, *Chem. Lett.*, 1987, 389.
9 M. Asami, *Bull. Chem. Soc. Jpn.*, 1990, **63**, 721.
10 D. Bhuniya and V. K. Singh, *Synth. Commun.*, 1994, **24**, 375.
11 D. Bhuniya and V. K. Singh, *Synth. Commun.*, 1994, **24**, 1475.
12 D. Bhuniya, A. DattaGupta and V. K. Singh, *Tetrahedron Lett.*, 1995, **36**, 2847.
13 D. Bhuniya, A. DattaGupta and V. K. Singh, *J. Org. Chem.*, 1996, **61**, 6108.
14 M. Asami, T. Suga, K. Honda and S. Inoue, *Tetrahedron Lett.*, 1997, **38**, 6425.
15 J. P. Tierney, A. Alexakis and P. Mangeney, *Tetrahedron: Asymmetry*, 1997, **8**, 1019.
16 M. J. Södergren and P. G. Andersson, *J. Am. Chem. Soc.*, 1998, **120**, 10760.
17 M. J. Södergren, S. K. Bertilsson and P. G. Andersson, *J. Am. Chem. Soc.*, 2000, **112**, 6610.
18 R. I. Olsson and P. Ahlberg, *Tetrahedron: Asymmetry*, 1999, **10**, 3991.
19 A. Ramírez and D. B. Collum, *J. Am. Chem. Soc.*, 1999, **121**, 11114.
20 M. Majewski and P. Nowak, *Tetrahedron Lett.*, 1998, **39**, 1661.
21 S. O. Nilsson Lill, P. I. Arvidsson and P. Ahlberg, *Tetrahedron: Asymmetry*, 1999, **10**, 265.
22 E.-U. Würthwein, K. Behrens and D. Hoppe, *Chem. Eur. J.*, 1999, **5**, 3459.
23 P. I. Arvidsson, G. Hilmersson and P. Ahlberg, *J. Am. Chem. Soc.*, 1999, **121**, 1883.
24 M. Amedjkouh and P. Ahlberg, Poster presented at the 11th European Symposium on Organic Chemistry (ESOC 11), Göteborg, Sweden, July 23–28, 1999.
25 B. Colman, S. E. de Sousa, P. O'Brien, T. D. Towers and W. Watson, *Tetrahedron: Asymmetry*, 1999, **10**, 4175.
26 S. E. de Sousa, P. O'Brien and H. C. Steffens, *Tetrahedron Lett.*, 1999, **40**, 8423.
27 M. Amedjkouh, D. Pettersen, S. O. Nilsson Lill, Ö. Davidsson and P. Ahlberg, submitted for publication.
28 J. J. P. Stewart, *J. Comput. Chem.*, 1989, **10**, 209.
29 E. Anders, R. Koch and P. Freunscht, *J. Comput. Chem.*, 1993, **14**, 1301.
30 G. Hilmersson, P. I. Arvidsson, Ö. Davidsson and M. Håkansson, *J. Am. Chem. Soc.*, 1998, **120**, 8143.
31 A. Abbotto, A. Streitwieser and P. v. R. Schleyer, *J. Am. Chem. Soc.*, 1997, **119**, 11255.
32 E. Kaufmann, J. Gose and P. v. R. Schleyer, *Organometallics*, 1989, **8**, 2577.
33 K. M. Morgan and S. Gronert, *J. Org. Chem.*, 2000, **65**, 1461.
34 S. Morpurgo, M. Bossa and G. O. Morpurgo, *THEOCHEM*, 1998, **429**, 71.
35 D. Zhao, C.-y. Chen, F. Xu, L. Tan, R. Tillyer, M. E. Pierce and J. R. Moore, *Org. Synth.*, 2000, **77**, 12.
36 G. Miao and B. E. Rossiter, *J. Org. Chem.*, 1995, **60**, 8424.
37 W. J. Hehre, B. J. Deppmeier, A. J. Driessen, J. A. Johnson, P. E. Klunzinger, L. Lou, J. Yu, J. Baker, J. E. Carpenter, R. W. Dixon, S. S. Fielder, H. C. Johnson, S. D. Kahn, J. M. Leonard and W. J. Pietro, Spartan v. 5.0.1, Irvine, CA, 1997.
38 W. Huang, personal communication.
39 G. I. Csonka, *J. Comput. Chem.*, 1993, **14**, 895.
40 G. I. Csonka and J. G. Angyan, *J. Mol. Struct.*, 1997, **393**, 31.
41 A. D. Becke, *J. Chem. Phys.*, 1993, **98**, 5648.
42 C. Lee, W. Yang and R. G. Parr, *Phys. Rev. B.*, 1988, **37**, 785.
43 P. C. Hariharan and J. A. Pople, *Theor. Chim. Acta*, 1973, **28**, 213.
44 M. J. Frisch, J. A. Pople and J. S. Binkley, *J. Chem. Phys.*, 1984, **80**, 3265.
45 T. Clark, J. Chandrasekhar, G. W. Spitznagel and P. v. R. Schleyer, *J. Comput. Chem.*, 1983, **4**, 294.